Title: Potent synthetic nanobodies against SARS-CoV-2 and molecular basis for neutralization

Short title: Nanobody neutralizers for SARS-CoV-2

One sentence summary: Structural and biochemical studies revealed the molecular basis for the neutralization mechanism of *in vitro*-selected and rationally designed nanobody neutralizers for SARS-CoV-2 pseudovirus.

Authors: Tingting Li[1,#], Hongmin Cai[1,#], Hebang Yao[1,#], Bingjie Zhou[2,#], Yapei Zhao[2], Wenming Qin[3], Cedric A.J. Hutter[4], Yanling Lai[1], Juan Bao[1], Jiaming Lan[2], Gary Wong[2], Markus Seeger[4], Dimitri Lavillette[2,5*], Dianfan Li[1,*]

Affiliation: [1]State Key Laboratory of Molecular Biology, CAS Center for Excellence in Molecular Cell Science, National Center for Protein Science Shanghai, Shanghai Institute of Biochemistry and Cell Biology, University of Chinese Academy of Sciences, Chinese Academy of Sciences, 333 Haike Road, Shanghai 201210, China.

[2]CAS Key Laboratory of Molecular Virology & Immunology, Institut Pasteur of Shanghai, University of Chinese Academy of Sciences, Chinese Academy of Sciences, 320 Yueyang Road, Shanghai 200031, China.

[3]National Facility for Protein Science in Shanghai, Shanghai Advanced Research Institute (Zhangjiang Laboratory), Chinese Academy of Sciences, Shanghai, 201210, China.

[4]Institute of Medical Microbiology, University of Zurich, Zurich, Switzerland.

[5]Pasteurien College, Soochow University, Jiangsu, China.

[*]**Correspondence:** dianfan.li@sibcb.ac.cn; dlaville@ips.ac.cn

ABSTRACT

SARS-CoV-2, the Covid-19 causative virus, adheres to human cells through binding of its envelope Spike protein to the receptor ACE2. The Spike receptor-binding domain (S-RBD) mediates this key event and thus is a primary target for therapeutic neutralizing antibodies to mask the ACE2-interacting interface. Here, we generated 99 synthetic nanobodies (sybodies) using ribosome and phage display. The best sybody MR3 binds the RBD with K_D of 1.0 nM and neutralizes SARS-CoV-2 pseudovirus with IC_{50} of 0.40 μg mL^{-1}. Crystal structures of two sybody-RBD complexes reveal a common neutralizing mechanism through which the RBD-ACE2 interaction is competitively inhibited by sybodies. The structures allowed the rational design of a mutant with higher affinity and improved neutralization efficiency by ~24-folds, lowering the IC_{50} from 12.32 to 0.50 μg mL^{-1}. Further, the structures explain the selectivity of sybodies between SARS-CoV strains. Our work presents an alternative approach to generate neutralizers against newly emerged viruses.

INTRODUCTION

The coronavirus disease emerged in early December 2019 (Covid-19) is posing a global health crisis (*1*). First reported in Wuhan, China (*2*), the pneumonia disease has spread worldwide and caused an official number of >7 million infections and >400,000 death as of the middle of June 2020. The causative agent, named as severe acute respiratory syndrome coronavirus 2 (SARS-CoV-2), is the sixth coronavirus to cause human fatalities, among the previous SARS-CoV (*3*) and the Middle East respiratory syndrome (MERS)-CoV (*4, 5*). Compared to SARS-CoV, SARS-CoV-2 has evolutionally perfected for spreading with characteristics of lower fatality, higher transmitting efficiency, and higher occurrence of asymptomatic patients and hence higher risk for unknowing spread (*6*).

Prompt responses in the science community have shed mechanistic insights into its high infectivity. Much of it is associated with its Spike protein (S), a heavily glycosylated, homotrimeric type-I membrane protein on the viral envelop that makes the corona-shaped 'spikes' on the surface (*7, 8*). During the infection, S is cleaved by host proteases (*9, 10*), yielding the N-terminal S1 and the C-terminal S2 subunit. S1 binds to ACE2 (*11-14*) on the host cell membrane via its receptor-binding domain (RBD), causing conformational changes that triggers a secondary cleavage needed for the S2-mediated membrane fusion at the plasma membrane or in the endosome.. Several independent structural studies have revealed that the SARS-CoV-2 RBD binds the receptor ACE2 with a 10-20 times higher affinity than SARS-CoV (*11-13*). This, together with the fact that the SARS-CoV-2 S protein is more prone to proteolysis (*7, 15*), may explain its high infectivity.

Despite fast research actions and progress, currently, there is no clinically available vaccines or drugs against SARS-CoV-2. Developing therapeutics, including neutralizing antibodies, has been a high priority for research globally. Because of its key role for viral attachment, the RBD has been a primary target for neutralizing strategies to block its binding to ACE2. In the past, several neutralizing antibodies isolated from recovered SARS (*16-19*) and MERS (*19-21*) patients have been found to bind the RBD. Similarly, several neutralizing antibodies recently identified from convalescent plasma in several independent studies (*22-24*) have been shown to suppress viral entry by blocking the RBD-ACE2 interactions. Altogether, these results demonstrate the RBD is a hot-spot to generate effective neutralizers for SARS-CoV-2.

Single-domain antibodies (nanobodies) found in llama and sharks contain only the heavy chain, yet they can bind antigen with affinities similar to the conventional

antibodies (*25*). Because the variable fragment is small (~14 kDa), it may access regions that are sterically hindered for bulkier two-chain antibodies. Additionally, as monomers and normally nonglycosylated, nanobodies are generally more heat stable, easier to produce (can be produced in bacteria), and more amenable to protein engineering than conventional antibodies (*25*). Recently, three highly diverse libraries of synthetic nanobodies (sybodies) have been rationally designed. Compared to immunization, the selection from sybody libraries offers quicker selection, making it possible to obtain nano-molar affinity antibodies in 2-3 weeks (*26, 27*). This accelerated pace is most attractive in cases to develop antibodies against newly emerged and quick spreading diseases like Covid-19. In addition, unlike for the isolation of antibodies from recovered patients, the *in vitro* selection does not require access to high-level biosafety labs or hospital resources, enabling early-stage antibody discovery by a wider research community.

Here, we generated 99 unique sybodies against the SARS-CoV2 S-RBD from three libraries using a combination of ribosome display and phage display. The best sybody MR3 binds the RBD with a K_D of 1.0 nM and neutralizes SARS-CoV-2 pseudovirus with an IC_{50} of 0.40 μg mL^{-1}. We determined the structures of two sybody-RBD complexes, revealing that they block virus infection by competing with ACE2 for RBD-binding. The structures also enabled the rational design of an improved version of MR17, lowering the IC_{50} from 12.32 to 0.50 (μg mL^{-1}). Our results pave the way to the development of therapeutic nanobodies to fight Covid-19.

RESULTS AND DISCUSSION

Sybody selection against the SARS-CoV-2 receptor-binding domain

SARS-CoV-2 S-RBD binders were selected by performing one round of ribosome display using three high-diversity libraries (Concave, Loop, and Convex) (*26, 27*), and three rounds of phage display using the biotinylated RBD as the bait under increasingly stringent selection conditions with the last selection at 5 nM RBD. To eliminate binders with fast off-rates, libraries were challenged with the non-biotinylated RBD during the panning process (*27*). After panning, 95 colonies for each of the three libraries were screened by ELISA (**Fig. S1A**) with the unrelated maltose-binding protein (MBP) as a control. A 1.5-fold (RBD:MBP) signal cut-off identified 80, 77, and 90 positive clones, corresponding to 62, 19, and 18 unique binders from the Concave, Loop, and Convex library, respectively (**Table S1**). The high redundancy in the Loop and Convex library suggests that the panning strategy was strict and that binders from the last round were sampled adequately.

Remarkably, no overlap of binders was found between the current study and an independent parallel study with the same libraries (*28*) despite that both studies reported internal redundancy. It is noted that the two studies used slightly different constructs and strategies; still, this statistically unexpected non-overlap reflects the high diversity of the synthetic sybody libraries.

Eighty 'first-comers' of the sequencing results for the 247 ELISA-positive colonies were further screened by a fluorescence-detector size exclusion chromatography (FSEC) assay to identify sybodies that can bind the RBD at a low concentration of 500 nM using crude extract from sybody-expressing clones. The assay identified 9 Concave (21%), 9 Loop (50%), and 10 Convex (56%) sybodies that caused earlier retention of the fluorescein-labeled RBD (**Fig. S2A-2D, Table S1**). Overall, the FSEC-positive clones numbered 28 (36%). Although the Concave pool was more diverse, it had the lowest positive rate.

We picked 9 FSEC-positive sybodies with various ELISA-redundancies for preparative purification (**Fig. S2E-2H**) and crystallization. They include SR4 (1), SR34 (2), SR38 (2), MR3 (31), MR4 (9), MR6 (3), MR17 (1), LR1 (31), and LR5 (19) (S, M, L refers to Concave, Loop, and Convex sybodies respectively; brackets indicate ELISA redundancy). All sybodies co-eluted with the RBD ((**Fig. S2E-2H**), confirming the formation of sybody-RBD complexes. Based on the crystallization outcome (**Fig. S3**), four sybodies, namely SR4, MR3, MR4, and MR17, were selected for biochemical characterization.

As designed (*26*), the four sybodies all displayed ultra-high thermostability (**Fig. 1, Fig. S4**). This could mean prolonged shelve life should they be useful for medical applications. The binding kinetics between sybodies and the RBD was assessed using bio-layer interferometry (*29*). As shown in **Fig. 1**, the K_D values ranged from 83.7 nM (MR17) to 1.0 nM (MR3). Consistent with its highest affinity, MR3 showed the slowest off-rate (2.3×10^{-4} s^{-1}). Taken together, the selection strategy yielded high-affinity binders that were ultra-stable.

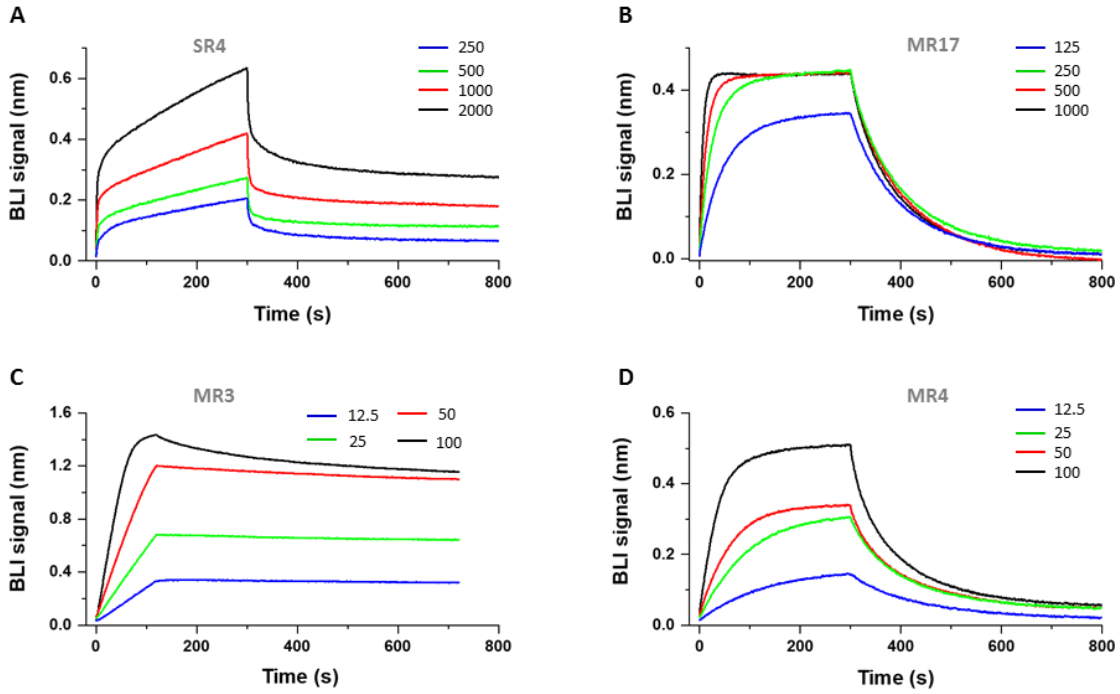

E

Sybody	Yield (mg L^{-1})	Fractional FL ($_{99\,°C\,/\,4°C}$)	K_D (nM)	K_{on}, $M^{-1}\,s^{-1}$	K_{off}, s^{-1}	IC_{50} (μg mL^{-1})
SR4	16.3	0.58	14.5	9.9×10^4	1.4×10^{-3}	5.90
MR17	20.2	0.80	83.7	1.2×10^5	9.7×10^{-3}	12.32
MR3	18.8	0.70	1.0	2.3×10^5	2.3×10^{-4}	0.40
MR4	29.7	0.73	23.3	2.7×10^5	6.4×10^{-3}	0.74

Fig. 1. Characterization of RBD nanobody binders. (**A-D**) Kinetics for sybody-RBD binding by bio-layer interferometry (BLI) assay. Biotinylated RBD immobilized on a streptavidin-coated sensor was titrated with various concentrations (nM) of sybodies as indicated. Data were fitted using the built-in software Data Analysis 10.0 with a 1:1 stoichiometry. (**E**) A summary of the characterization of the four sybodies. Yield refers to the amount of pure sybodies from 1 L of culture. Fractional fluorescence (FL) indicates remaining gel filtration peak intensity of sybodies after heating at 99 °C for 20 min (**Fig. S4A-4D**). The binding kinetics are from (**A-D**). IC_{50} values are from **Fig. 2**.

Neutralizing activity of sybodies

We next tested the capacity of sybodies to inhibit entry of retroviral pseudotypes harboring the SARS-CoV-2 Spike protein. Using 50% neutralization at 1 μM concentration as a cut-off, 11 Concave (26%), 13 Loop (68%), and 10 Convex (56%) sybodies were identified as positive (**Fig. S5A**). Thus, nearly a half of the tested sybodies showed neutralizing activity against SARS-CoV-2 pseudovirus according to

the abovementioned criterion. Interestingly, none of the sybodies showed noticeable neutralization activities for the closely related SARS-CoV pseudovirus (**Fig. S5B**), indicating high specificity.

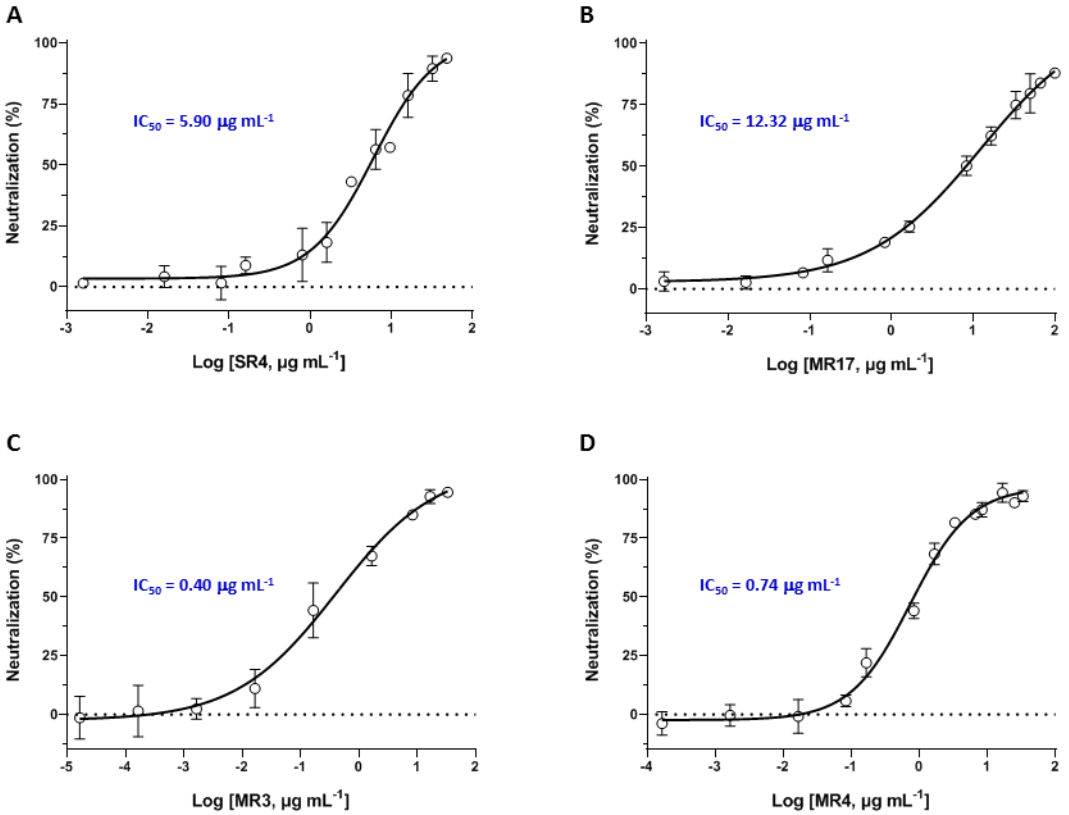

Fig. 2. Neutralization activity of sybodies against SARS-CoV-2 pseudovirus. (**A-D**) Pseudoviral particles were preincubated with different concentration of indicated sybodies before infection of VeroE6-hACE2 cells. The rate of infection was measure by fluorescence-activated cell sorting (FACS). IC_{50} was obtained by Sigmoid fit of the percentage neutralization. Data are from three independent experiments.

Although the number of ELISA hits was less in the Loop and Convex libraries (**Fig. S1**), the positive rate for neutralization was much higher than the Concave library – a consistent trend observed in the FSEC analysis (**Table S1**). It is possible that, for the Concave library, the panning conditions were not strict enough to eliminate binders with high-off rates or low affinities. This would justify a stricter panning process for the Concave library to increase the quality of the binders at the cost of diversity. Alternatively, the Concave sybodies may intrinsically be different from the other two pools and they may have preference for some other epitopes not overlapping with the ACE-binding site.

IC_{50} values of the four sybodies were determined to be 5.90 μg mL^{-1} for SR4, 12.32 μg mL^{-1} for MR17, 0.40 μg mL^{-1} for MR3, and 0.74 μg mL^{-1} for MR4 (**Fig. 2**).

Crystal structure of two sybody-RBD complexes

To elucidate the molecular basis for neutralization, we set to determine the structures for the four RBD-sybody complexes using X-ray crystallography. MR4-RBD crystals formed clustered needles (**Fig. S3**) and were not tested. Crystals for MR3-RBD, even after several rounds of optimization with multiple constructs (myc-tagged, tagless (*26*), and a recently reported "macrobody" version of MBP-fusion (*30*)), did not diffract beyond 7 Å. Therefore, the focus for structural studies was shifted to SR4 and MR17.

Crystals for SR4-RBD and MR17-RBD yielded data sets at 2.15 Å and 2.77 Å, respectively (**Table S2**). The structures were solved using molecular replacement with the published RBD structure (PDB ID 6M0J) (*11*) and a sybody structure (PDB ID 5M13) (*26*) as search models. The SR4-RBD and MR17-RBD structures were refined to R_{work}/R_{free} of 0.1836/0.2239 and 0.2029/0.2659, respectively. The asymmetric unit contained one RBD and one sybody molecule for both complexes, meaning a 1:1 stoichiometry which was consistent with the bio-layer interferometry results.

The RBD structure resembles a short backrest high chair and SR4 binds to it at both the seat and backrest part (**Fig. 3A**). A PISA (*31*) analysis showed a 727.37 $Å^2$ surface area for the SR4-RBD interface with modest electrostatic complementarity (**Fig. 3A**, **Fig. S6A**). Structural alignment of the SR4-RBD complex with the RBD-ACE2 crystal structure revealed that SR4-binding did not cause noticeable conformational changes of the RBD (**Fig. S7**) with the RMSD value of 0.370 Å. All three CDRs contributed to the binding through hydrophobic interactions and H-bonding that involves both sidechains and mainchains (**Fig. 3B, 3C**). In addition, Tyr37, which is at the framework region, also participated binding by forming an H-bond with the RBD Gly447 backbone. Of note, SR4 binds sideways, as intended by design of the Concave sybody library (*26*).

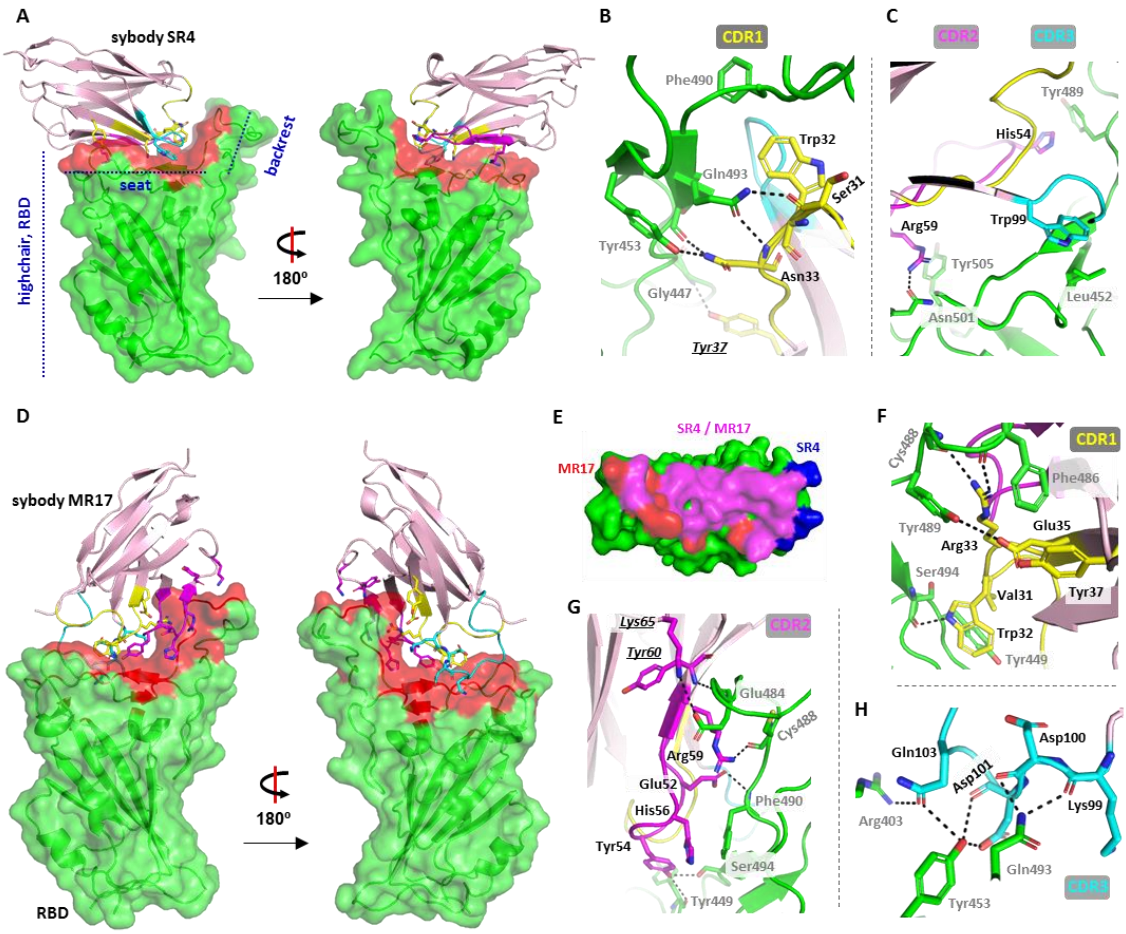

Fig. 3. Crystal structure of two sybody-RBD complexes. (**A**) The overall structure of SR4 (pink cartoon) bound with RBD (green surface) which resembles a short backrest high chair. The binding surface is highlighted red. (**B,C**) Interactions between SR4 and the RBD (green) contributed by CDR1 (yellow), CDR2 (magenta), and CDR3 (cyan). The framework residue Tyr37 involved in the interactions is shown underlining italic. (**D**) The overall structure of the MR17-RBD complex. Color-coding is the same as in **A**. (**E**) The overlap between the SR4- and MR17-interacting surfaces. (**F-H**). Interactions between MR17 and the RBD (green) contributed by CDR1 (yellow), CDR2 (magenta), and CDR3 (cyan). The framework Lys65 and Tyr60 participated in the binding are shown underling italic. Dashed lines indicate H-bonding or salt-bridges between atoms that are <4.0 Å apart. Labels for sybody residues are colored black and labels for the RBD residues are colored grey.

MR17 also binds to the RBD at the 'seat' and 'backrest' regions but approaches the RBD an almost perfect opposite direction of SR4 (**Fig. 3D, Fig. S8**), indicating divergent binding mode for these synthetic nanobodies. The binding of MR17 to the

RBD occurred on a 853.94 Å^2 surface area with noticeable electrostatic complementarity (**Fig. S6B**). Interestingly, this surface was largely shared with the SR4 binding surface (**Fig. 3E**). Similar to SR4, MR17 did not cause noticeable conformational changes of the RBD (RMSD of 0.508 Å) (**Fig. S7**), except for a small flip at the 'backrest' part of the RBD. The interactions between MR17 and the RBD were mainly mediated by H-bonding (**Fig. 3F-3H**). Apart from the three CDRs, the framework Lys65 and Tyr60 participated in RBD-binding by salt-bridging with the sidechain and H-bonding with the mainchain of Glu484, respectively.

Molecular basis for neutralization

Neutralizing antibodies may interact with different parts of the S protein and thus blocks viral entry through different mechanisms (*7, 19, 22, 23, 32*). Because the current project was designed to select sybodies against the receptor-binding domain of S protein, the neutralizers were expected to suppress ACE2 binding by competing for the binding surface, by steric hindrance for ACE2 binding, or by deforming the ACE2 binding surface. Superposing the structure of the sybody-RBD complexes to the RBD-ACE2 (PDB ID 6M0J) (*11*) revealed that they both bind the RBD at the interface where the receptor ACE2 binds (**Fig. 4A, 4B**). Aligning the sybody-RBD structures to the full-length S protein (*7*) showed no steric hindrance for the sybody in binding to the 'up' conformation of the RBD in the 'open' prefusion state of S protein (**Fig. 4C, 4D**). In addition, the sybodies may be able to bind S protein in its 'closed' state due to their small sizes. Indeed, little clashes were observed when SR4/MR17 were aligned onto the S protein in its 'closed' conformation (**Fig. S9**).

Consistent with the structural observations, the RBD-ACE2 binding can be disrupted by sybodies SR4, MR17, MR3, and MR4 to various degrees (**Fig. 4E-4H**). Therefore, we conclude that SR4/MR17, and perhaps MR3/MR4 too, block the viral entry by masking the ACE2-binding surface of the RBD thus preventing the recognition between viral particles and host cells.

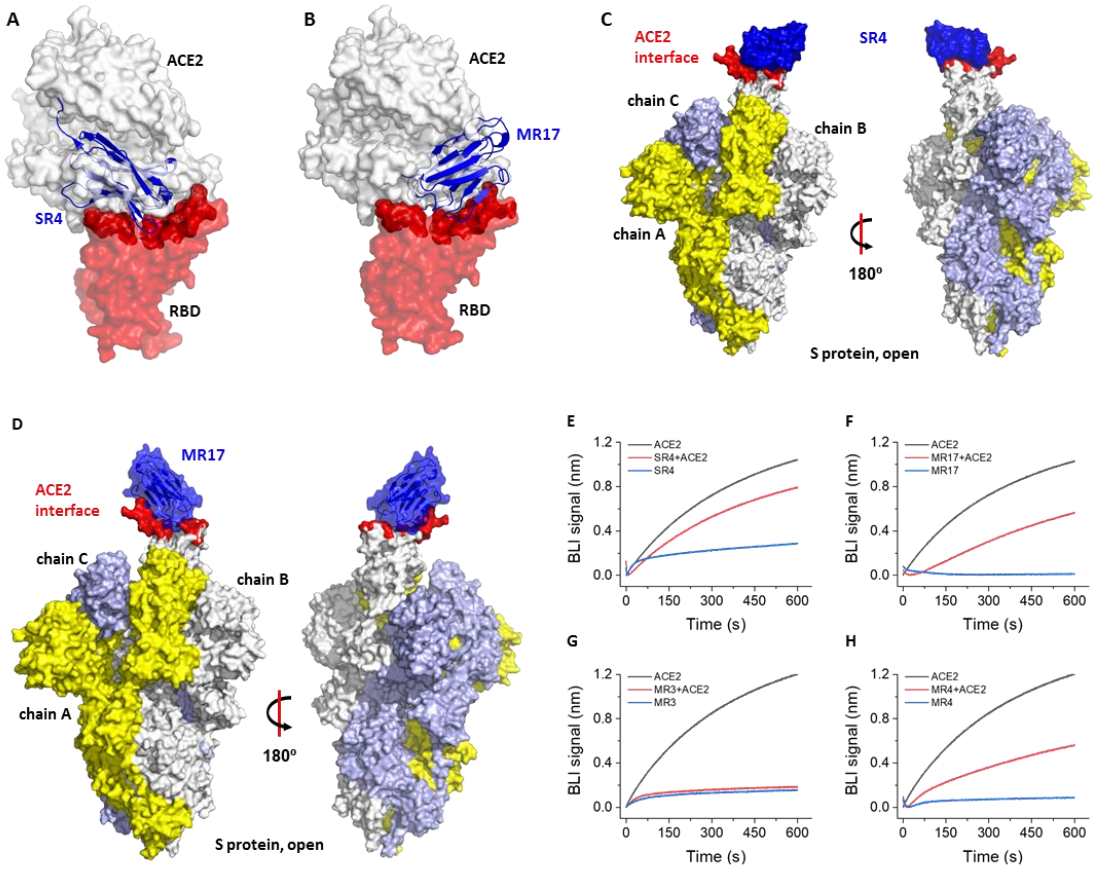

Fig. 4. Molecular basis for neutralization. (**A**) Alignment of the SR4-RBD structure to the ACE2-RBD structure (PDB ID 6M0J) (*11*) reveals that SR4 (blue) binds RBD (red) at the ACE2-binding site (dark red). The receptor ACE2 is shown as a white surface. (**B**) Alignment of the SR4-RBD structure to the ACE2-RBD structure (PDB ID 6M0J) (*11*) reveals that MR17 binds the RBD at the ACE2-binding site. The color coding is the same as in **A**. (**C,D**) Alignment of the SR4-RBD (**C**) and MR17-RBD (**D**) to the 'up' conformation of the RBD from the cryo-EM structure of the full-length S protein (PDB ID 6VYB) (*7*). (**E-H**) Competitive binding for the RBD between sybody and ACE2. A sensor coated with streptavidin was saturated with 1 μM of biotinylated RBD. The sensor was then soaked in 50 nM of sybody with (red) or without 25 nM of ACE2 (blue) for bio-layer interferometry (BLI) assays. As a control, the ACE2-RBD interaction was monitored using sensors without sybody incubation (black).

An improved MR17 mutant by structure-based design

The neutralizing activity of MR17 was modest (IC_{50} of 12.32 μg mL^{-1}, **Fig. 2B**). To improve its neutralizing potency, we designed 19 single mutants based on the MR17-RBD structure (see Methods). A neutralization assay identified K99Y with higher potency than the wild-type MR17 (**Fig. S10**), and the rationale for its design is

described below. As shown in **Fig. 3H**, few hydrophobic interactions were observed between MR17 and the RBD even though 5 of the 12 amino acids in the CDR3 are hydrophobic (K^{99}DDGQLAYHYDY^{110}, hydrophobic residues are underlined). Intriguingly, the RBD contains a hydrophobic patch at where CDR3 was oriented; and this patch is adjacent to an overall positively-charged surface (**Fig. 5A**). However, the MR17 residue poking into this patch is a positively charged residue, namely Lys99 (**Fig. 5B**) which would be unfavorable because of electrostatic repel and/or hydrophobic-hydrophilic repel. Thus, it was proposed that a hydrophobic replacement should strengthen the interactions. According to the original library design, Lys99 was unvaried (*26*), meaning that Lys99 was not *selected* and hence offering opportunities for optimization. The analysis encouraged the design of the K99Y mutation to match this hydrophobic microenvironment.

As shown in **Fig. 5C**, the single mutation increased the binding affinity by 1.5 fold and decreased the off-rate by 2.8 fold. Consistent with this trend, MR17-K99Y displayed a remarkable 24-fold increase of neutralization efficiency, with an IC_{50} value (0.50 μg mL^{-1}) (**Fig. 5D**) comparable to the best sybody MR3 (**Fig. 1E, Fig. 2C**). As expected, Tyr99 was indeed in close contact with the hydrophobic patch, as revealed by the crystal structure of MR17-K99Y (**Fig. 5E, Table S2**). Based on the improvements, we further designed K99W. K99W showed similar neutralization activities with the wild-type MR17 (**Fig. S10**); it may be that the bulky side chain of tryptophan caused clashes with the hydrophobic pocket. Altogether, the mutagenesis work not only yielded to an improved neutralizing sybody but also provided validation of the structure and neutralization mechanism of MR17.

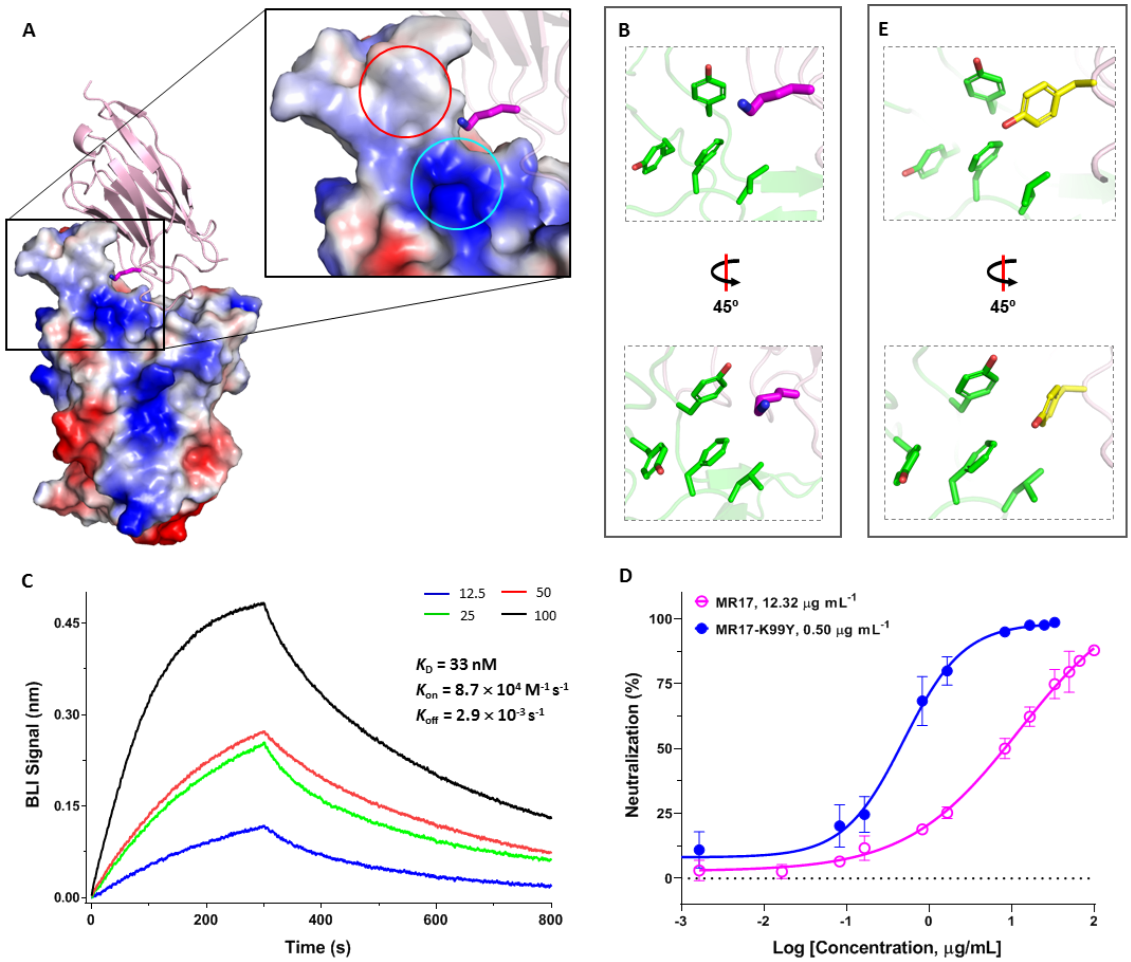

Fig. 5. Rational design of a sybody mutant with increased RBD binding affinity and higher neutralizing activity. (**A**) The overall structure and the expanded view of MR17 (pink cartoon) in complex with the RBD (electrostatic surface). Lys99 on CDR3 (magenta carbon atoms) is poking to an overall positively charged area (cyan circle) which is also adjacent to a hydrophobic patch (red circle). (**B**) Lys99 from MR17 (magenta) is situated in a hydrophobic patch. (**C**) Binding kinetics between MR17-K99Y and the RBD. Biotinylated RBD immobilized on a streptavidin-coated sensor was titrated with various concentrations (nM) of MR17-K99Y as indicated. Data were fitted using the built-in software Data Analysis 10.0 with a 1:1 stoichiometry. (**D**) Neutralization assay of MR17-K99Y (closed circle) using SARS-CoV-2 pseudovirus shows improved neutralizing efficiency compared to the MR17 wild-type (open circle). Data are from three independent experiments. (**E**) Crystal structure of MR17-K99Y shows that Tyr99 matches the hydrophobic microenvironment.

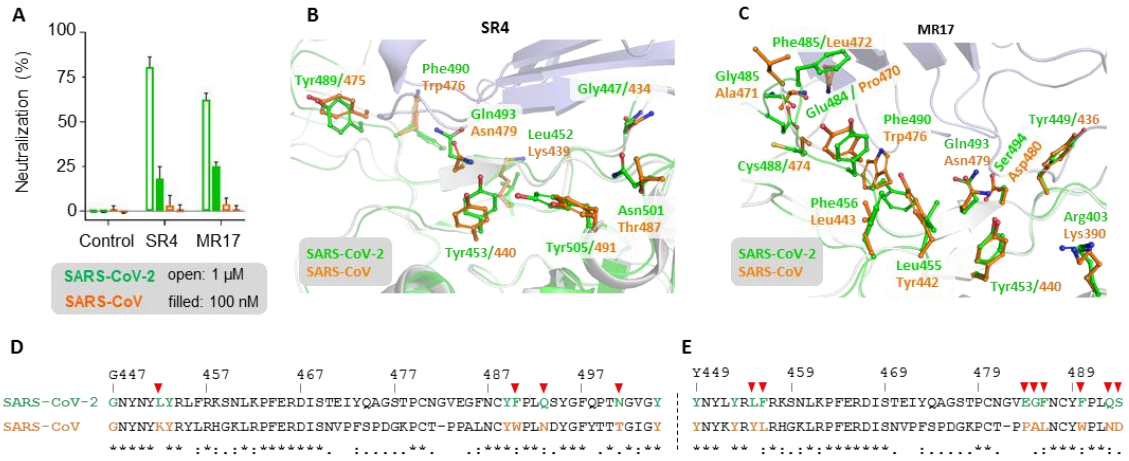

Fig. 6. Structural basis for neutralization selectivity. (**A**) Selectivity of the SR4 and MR17 in neutralizing the two SARS-CoV pseudoviruses. Neutralization assays were conducted using SARS-CoV (magenta) and SARS-CoV-2 (green) pseudotypes with 2 concentrations of sybodies (1 μM and 100 nM). Error bar represents standard deviation of data from three independent experiments. (**B, C**) The structure of SR4-RBD (**B**) and MR17-RBD (**C**) are aligned to the SARS-CoV RBD in a neutralizer-bound form (*16*). SR4 is shown as light blue cartoon. The SARS-CoV-2 RBD is colored green. The SARS-CoV RBD is shown as white cartoon with the aligned residues shown as orange sticks. (**D,E**) Sequence alignment between the two RBDs from SARS-CoV-2 and SARS-CoV in the epitope for SR4 (**D**) and MR17 (**E**). Residues from the SARS-CoV-2 RBD are numbered above the sequence. The SARS-CoV-2 RBD residues involved in the binding are colored green, and the corresponding residues in the SARS-CoV RBD are colored orange, as in **B** and **C**. Red triangles above the sequence indicate differences between the two RBDs in the epitope. Asterisks mark identical residues, colons refer to conserved residues, and single dots indicate modestly conserved residues.

Structural basis for neutralization specificity

Cross-activities of neutralizing activities have been reported for antibodies between SARS-CoV and SARS-CoV-2 (*7, 33, 34*) because the S-RBDs from the two viruses are highly similar, with 74.3% identify and 81.7 % similarity. However, none of the SARS-CoV-2 sybody neutralizers (**Fig. 6A, Fig. S5, Fig. S10**) showed noticeable neutralizing activity for SARS-CoV, even at 1 μM concentration. To find out structural mechanisms for the functional selectivity, we compared the SARS-CoV-2 RBD structures in SR4- and MR17-bound form with the SARS-CoV RBD also in a neutralizer-binding form (PDB ID 2dd8) (*16*). Although the two RBDs are overall very similar (**Fig. S11**), the residues involved in sybody recognition are not conserved between the two

(**Fig. 6B-6E**). Specifically, half of the eight SR4-interacting residues and 9 of 12 MR17-interacting residues are different between the two RBDs. Although some of these residues interacted with the sybodies via their mainchain amides and carbonyls, the side chain differences can still cause slight changes in mainchain orientation. Because nanobodies mostly recognize three-dimensionally organized epitopes (as was the case here) and the recognition is conformation sensitive, such small changes might be enough to diminish antibody-antigen interactions, thus leading to the observed selectivity.

In summary, we have generated potent synthetic nanobodies which neutralize SARS-CoV-2 pseudoviruses efficiently and selectively. We anticipate the selection strategy be useful to quickly respond to similar crises should they arise in the future.

ACKNOWLEDGMENTS

We thank the staff members of the Large-scale Protein Preparation System for equipment maintenance and management. We thank Dr. Zhipu Luo at Soochow University (China) for helpful discussions regarding data processing. This work has been supported by the Key Program of CAS Frontier Science (QYZDB-SSW-SMC037, D.Li), the Strategic Priority Research Program of the Chinese Academy of Sciences (XDB37020204, D.Li), CAS Facility-based Open Research Program, the National Natural Science Foundation of China (31870726, D.Li), the One Belt and One Road major project for infectious diseases (2018ZX10101004-003, J.L.), National Key R&D Program of China (2020YFC0845900, D.La), and Shanghai Municipal Science and Technology Major Project (20431900402, D.La).

AUTHOR CONTRIBUTIONS

T.L., H.C., and H.Y. selected sybodies under the supervision of C.A.J.H. and M.A.S.. T.L., H.C., and H.Y. purified and crystalized protein complexes with assistance from Y.L.. H.Y. biochemically characterized sybodies. B.Z. and Y.Z. performed neutralization assays under the supervision of D.La. W.Q. collected X-ray diffraction data. B.J. helped with molecular cloning. J.L. and G.W. developed reagents for the neutralizing assays. D.Li. conceived the project, solved the structures, analyzed data, and wrote the manuscript with inputs from H.Y., T.L., H.C., B.Z., M.A.S., and D.La.

CONFLICT OF INTEREST

The authors declare no conflict of interest.

REFERENCES

1. M. Nicola, Z. Alsafi, C. Sohrabi, A. Kerwan, A. Al-Jabir, C. Iosifidis, M. Agha, R. Agha, The socio-economic implications of the coronavirus pandemic (COVID-19): A review. *Int J Surg* **78**, 185-193 (2020).
2. C. Wang, P. W. Horby, F. G. Hayden, G. F. Gao, A novel coronavirus outbreak of global health concern. *Lancet* **395**, 470-473 (2020).
3. J. S. M. Peiris, K. Y. Yuen, A. D. M. E. Osterhaus, K. Stöhr, The Severe Acute Respiratory Syndrome. *N Engl J Med* **349**, 2431-2441 (2003).
4. M. Z. Tay, C. M. Poh, L. Rénia, P. A. MacAry, L. F. P. Ng, The trinity of COVID-19: immunity, inflammation and intervention. *Nat Rev Immunol* **20**, 363-374 (2020).
5. D. S. Hui, Tracking the transmission and evolution of MERS-CoV. *Lancet* **382**, 1962-1964 (2013).
6. K.-S. Yuen, Z.-W. Ye, S.-Y. Fung, C.-P. Chan, D.-Y. Jin, SARS-CoV-2 and COVID-19: The most important research questions. *Cell Biosci* **10**, 40-40 (2020).
7. A. C. Walls, Y.-J. Park, M. A. Tortorici, A. Wall, A. T. McGuire, D. Veesler, Structure, Function, and Antigenicity of the SARS-CoV-2 Spike Glycoprotein. *Cell* **181**, 281-292.e286 (2020).
8. D. Wrapp, N. Wang, K. S. Corbett, J. A. Goldsmith, C.-L. Hsieh, O. Abiona, B. S. Graham, J. S. McLellan, Cryo-EM structure of the 2019-nCoV spike in the prefusion conformation. *Science* **367**, 1260-1263 (2020).
9. J. Shang, Y. Wan, C. Luo, G. Ye, Q. Geng, A. Auerbach, F. Li, Cell entry mechanisms of SARS-CoV-2. *Proc Natl Acad Sci USA* **117**, 11727-11734 (2020).
10. M. Hoffmann, H. Kleine-Weber, S. Schroeder, N. Krüger, T. Herrler, S. Erichsen, T. S. Schiergens, G. Herrler, N.-H. Wu, A. Nitsche, M. A. Müller, C. Drosten, S. Pöhlmann, SARS-CoV-2 Cell Entry Depends on ACE2 and TMPRSS2 and Is Blocked by a Clinically Proven Protease Inhibitor. *Cell* **181**, 271-280.e278 (2020).
11. J. Lan, J. Ge, J. Yu, S. Shan, H. Zhou, S. Fan, Q. Zhang, X. Shi, Q. Wang, L. Zhang, X. Wang, Structure of the SARS-CoV-2 spike receptor-binding domain bound to the ACE2 receptor. *Nature* **581**, 215-220 (2020).
12. J. Shang, G. Ye, K. Shi, Y. Wan, C. Luo, H. Aihara, Q. Geng, A. Auerbach, F. Li, Structural basis of receptor recognition by SARS-CoV-2. *Nature* **581**, 221-224 (2020).
13. Q. Wang, Y. Zhang, L. Wu, S. Niu, C. Song, Z. Zhang, G. Lu, C. Qiao, Y. Hu, K.-Y. Yuen, Q. Wang, H. Zhou, J. Yan, J. Qi, Structural and Functional Basis of SARS-CoV-2 Entry by Using Human ACE2. *Cell* **181**, 894-904.e899 (2020).
14. R. Yan, Y. Zhang, Y. Li, L. Xia, Y. Guo, Q. Zhou, Structural basis for the recognition of SARS-CoV-2 by full-length human ACE2. *Science* **367**, 1444-1448 (2020).
15. M. Hoffmann, H. Kleine-Weber, S. Pöhlmann, A Multibasic Cleavage Site in the Spike

Protein of SARS-CoV-2 Is Essential for Infection of Human Lung Cells. *Mol Cell* **78**, 779-784.e775 (2020).

16. P. Prabakaran, J. Gan, Y. Feng, Z. Zhu, V. Choudhry, X. Xiao, X. Ji, D. S. Dimitrov, Structure of severe acute respiratory syndrome coronavirus receptor-binding domain complexed with neutralizing antibody. *The Journal of biological chemistry* **281**, 15829-15836 (2006).
17. E. Traggiai, S. Becker, K. Subbarao, L. Kolesnikova, Y. Uematsu, M. R. Gismondo, B. R. Murphy, R. Rappuoli, A. Lanzavecchia, An efficient method to make human monoclonal antibodies from memory B cells: potent neutralization of SARS coronavirus. *Nat Med* **10**, 871-875 (2004).
18. B. Rockx, D. Corti, E. Donaldson, T. Sheahan, K. Stadler, A. Lanzavecchia, R. Baric, Structural basis for potent cross-neutralizing human monoclonal antibody protection against lethal human and zoonotic severe acute respiratory syndrome coronavirus challenge. *J Virol* **82**, 3220-3235 (2008).
19. A. C. Walls, X. Xiong, Y.-J. Park, M. A. Tortorici, J. Snijder, J. Quispe, E. Cameroni, R. Gopal, M. Dai, A. Lanzavecchia, M. Zambon, F. A. Rey, D. Corti, D. Veesler, Unexpected Receptor Functional Mimicry Elucidates Activation of Coronavirus Fusion. *Cell* **176**, 1026-1039.e1015 (2019).
20. D. Corti, N. Passini, A. Lanzavecchia, M. Zambon, Rapid generation of a human monoclonal antibody to combat Middle East respiratory syndrome. *J Infect Public Heal* **9**, 231-235 (2016).
21. P. Niu, S. Zhang, P. Zhou, B. Huang, Y. Deng, K. Qin, P. Wang, W. Wang, X. Wang, J. Zhou, L. Zhang, W. Tan, Ultrapotent Human Neutralizing Antibody Repertoires Against Middle East Respiratory Syndrome Coronavirus From a Recovered Patient. *J Infect Dis* **218**, 1249-1260 (2018).
22. Y. Wu, F. Wang, C. Shen, W. Peng, D. Li, C. Zhao, Z. Li, S. Li, Y. Bi, Y. Yang, Y. Gong, H. Xiao, Z. Fan, S. Tan, G. Wu, W. Tan, X. Lu, C. Fan, Q. Wang, Y. Liu, C. Zhang, J. Qi, G. F. Gao, F. Gao, L. Liu, A noncompeting pair of human neutralizing antibodies block COVID-19 virus binding to its receptor ACE2. *Science*, eabc2241 (2020).
23. Y. Cao, B. Su, X. Guo, W. Sun, Y. Deng, L. Bao, Q. Zhu, X. Zhang, Y. Zheng, C. Geng, X. Chai, R. He, X. Li, Q. Lv, H. Zhu, W. Deng, Y. Xu, Y. Wang, L. Qiao, Y. Tan, L. Song, G. Wang, X. Du, N. Gao, J. Liu, J. Xiao, X.-d. Su, Z. Du, Y. Feng, C. Qin, C. Qin, R. Jin, X. S. Xie, Potent neutralizing antibodies against SARS-CoV-2 identified by high-throughput single-cell sequencing of convalescent patients' B cells. *Cell*, (2020).
24. B. Ju, Q. Zhang, J. Ge, R. Wang, J. Sun, X. Ge, J. Yu, S. Shan, B. Zhou, S. Song, X. Tang, J. Yu, J. Lan, J. Yuan, H. Wang, J. Zhao, S. Zhang, Y. Wang, X. Shi, L. Liu, J. Zhao, X. Wang, Z. Zhang, L. Zhang, Human neutralizing antibodies elicited by SARS-CoV-2 infection. *Nature*, (2020).

25. S. Muyldermans, Nanobodies: Natural Single-Domain Antibodies. *Annu Rev Biochem* **82**, 775-797 (2013).
26. I. Zimmermann, P. Egloff, C. A. J. Hutter, F. M. Arnold, P. Stohler, N. Bocquet, M. N. Hug, S. Huber, M. Siegrist, L. Hetemann, J. Gera, S. Gmür, P. Spies, D. Gygax, E. R. Geertsma, R. J. P. Dawson, M. A. Seeger, Synthetic single domain antibodies for the conformational trapping of membrane proteins. *eLife* **7**, e34317 (2018).
27. I. Zimmermann, P. Egloff, C. A. J. Hutter, B. T. Kuhn, P. Bräuer, S. Newstead, R. J. P. Dawson, E. R. Geertsma, M. A. Seeger, Generation of synthetic nanobodies against delicate proteins. *Nat Protoc* **15**, 1707-1741 (2020).
28. J. D. Walter, C. A. J. Hutter, I. Zimmermann, J. Earp, P. Egloff, M. Sorgenfrei, L. M. Hürlimann, I. Gonda, G. Meier, S. Remm, S. Thavarasah, P. Plattet, M. A. Seeger, Synthetic nanobodies targeting the SARS-CoV-2 receptor-binding domain. *bioRxiv*, 2020.2004.2016.045419 (2020).
29. Y. Abdiche, D. Malashock, A. Pinkerton, J. Pons, Determining kinetics and affinities of protein interactions using a parallel real-time label-free biosensor, the Octet. *Anal Biochem* **377**, 209-217 (2008).
30. J. D. Brunner, R. P. Jakob, T. Schulze, Y. Neldner, A. Moroni, G. Thiel, T. Maier, S. Schenck, Structural basis for ion selectivity in TMEM175 K+ channels. *eLife* **9**, e53683 (2020).
31. E. Krissinel, K. Henrick, Inference of Macromolecular Assemblies from Crystalline State. *J Mol Biol* **372**, 774-797 (2007).
32. X. Chi, R. Yan, J. Zhang, G. Zhang, Y. Zhang, M. Hao, Z. Zhang, P. Fan, Y. Dong, Y. Yang, Z. Chen, Y. Guo, J. Zhang, Y. Li, X. Song, Y. Chen, L. Xia, L. Fu, L. Hou, J. Xu, C. Yu, J. Li, Q. Zhou, W. Chen, A potent neutralizing human antibody reveals the N-terminal domain of the Spike protein of SARS-CoV-2 as a site of vulnerability. *bioRxiv*, 2020.2005.2008.083964 (2020).
33. M. Yuan, N. C. Wu, X. Zhu, C.-C. D. Lee, R. T. Y. So, H. Lv, C. K. P. Mok, I. A. Wilson, A highly conserved cryptic epitope in the receptor binding domains of SARS-CoV-2 and SARS-CoV. *Science* **368**, 630-633 (2020).
34. D. Wrapp, D. De Vlieger, K. S. Corbett, G. M. Torres, N. Wang, W. Van Breedam, K. Roose, L. van Schie, M. Hoffmann, S. Pöhlmann, B. S. Graham, N. Callewaert, B. Schepens, X. Saelens, J. S. McLellan, Structural Basis for Potent Neutralization of Betacoronaviruses by Single-Domain Camelid Antibodies. *Cell* **181**, 1004-1015.e1015 (2020).